Isotopic dependence of fusion cross sections in reactions with heavy nuclei

G.G.Adamian[1,2,3], N.V.Antonenko[1,2], W.Scheid[1]
[1]*Institut für Theoretische Physik der Justus–Liebig–Universität, D–35392 Giessen, Germany*
[2]*Joint Institute for Nuclear Research, 141980 Dubna, Russia*
[3]*Institute of Nuclear Physics, Tashkent 702132, Uzbekistan*
(February 9, 2008)

Abstract

The dependence of fusion cross section on the isotopic composition of colliding nuclei is analysed within the dinuclear system concept for compound nucleus formation. Probabilities of fusion and surviving probabilities, ingredients of the evaporation residue cross sections, depend decisively on the neutron numbers of the dinuclear system. Evaporation residue cross sections for the production of actinides and superheavy nuclei, listed in table form, are discussed and compared with existing experimental data. Neutron-rich radioactive projectiles are shown to lead to similar fusion cross sections as stable projectiles.

PACS:25.70.Jj, 24.10.-i, 24.60.-k
Key words: Complete fusion; Quasi–fission; Compound nucleus; Superheavy nuclei; Dinuclear system

The synthesis of superheavy elements (Z=106-112) was reached by cold fusion of heavy ions with lead and bismuth targets [1,2]. Hot fusion reactions using ^{232}Th, ^{238}U and ^{242,244}Pu targets were also applied to synthesize the elements with Z=110, 112 and 114 [3]. A possible next step is to explore the synthesis of heaviest nuclei with radioactive beams [2,4,5]. Microscopical investigations of such planned experiments are a challenge for theory. Usually the surviving probability W_{sur} of the formed compound nucleus against fission in the de–excitation process is considered as the crucial factor which is mainly responsible for producing heavy and superheavy elements. With neutron–reach projectiles one can obtain a large stability (large W_{sur}) of the compound nucleus. However, the probability of complete fusion P_{CN}, dependent on nuclear structure effects and on the neutron excess above the nearest closed shells in the colliding nuclei, is also very important for the correct calculation of the evaporation residue cross section σ_{ER}. For example, experimentally extracted probabilities P_{CN} are strongly decreased [6] when the neutron numbers of the projectile or target deviate from magic numbers.

The existing fusion models can be distinguished by their choice of the relevant collective degree of freedom responsible for complete fusion. Many models assume an adiabatic melting of the nuclei along the relative distance R of nuclear centers (or the elongation of the system) [7–12]. However, it was demonstrated that the adiabatic scenario of fusion along the relative distance leads to a large overestimation and an incorrect isotopic trend of the fusion probability [13]. The dinuclear system (DNS) concept [14–19] assumes that the united system is reached by a series of transfers of nucleons or small clusters from the light nucleus to the heavier one in a touching configuration. So, the dynamics of fusion is considered as a diffusion of the DNS in the mass asymmetry, defined by $\eta = (A_1 - A_2)/(A_1 + A_2)$ (A_1 and A_2 are the mass numbers the DNS nuclei), where the potential barrier $B^*_{\rm fus}$ in η supplies a hindrance for fusion.

The assumption of a touching configuration of the two reacting nuclei in the DNS model is supported by the structural forbiddenness of fusion [20,21] which hinders the nuclei to melt together along the relative distance. This aspect is phenomenologically described with a double folding potential in frozen density approximation which shows a minimum near the touching distance of the nuclei [22]. There are also experimental evidences [23,24] that the mass asymmetry degree of freedom equilibrates more rapidly than the elongation of the system. During the characteristic time of fusion a statistical approach is applicable to treat the evolution of the DNS which also includes a diffusion to larger relative distances between the centers of the nuclei describing the quasi–fission process (decay of the DNS) competing with the complete fusion. In reactions with heavy nuclei the quasi–fission channel dominates and leads to a strong reduction of the fusion [15–19].

In accordance with the DNS concept the evaporation residue cross section is factorized as follows [17]

$$\sigma_{ER}(E_{\rm cm}) = \sigma_c(E_{\rm cm}) P_{CN}(E_{\rm cm}, J=0) W_{sur}(E_{\rm cm}, J=0). \qquad (1)$$

The calculations of the evaporation residue cross sections demands an analysis of all three factors in (1). The value of σ_c is the effective capture cross section for the transition of the colliding nuclei over the entrance (Coulomb) barrier with the probability T:

$$\sigma_c(E_{\rm cm}) = \pi \lambda\!\!\!^{-2} (J_{max}+1)^2 T(E_{\rm cm}, J=0).$$

The contributing angular momenta in the evaporation residue cross section are limited by the surviving probability $W_{sur}(E_{\rm cm}, J)$ with $J_{max} \approx 10-20$ when highly fissile superheavy nuclei are produced [25]. This corresponds to almost central collisions with impact parameters smaller than 1 fm. The value of J_{max} is smaller than the critical angular momentum J_{crit} which restricts the capture cross section. For reactions leading to superheavy nuclei, values of $J_{max} = 10$ and $T(E_{\rm cm}, J = 0) = 0.5$ are chosen for energies $E_{\rm cm}$ near the Coulomb barrier. The capture cross sections obtained with these parameters are in agreement with the ones calculated within a microscopical model [18].

The probability of complete fusion P_{CN} in (1) depends on the competition between complete fusion and quasi–fission after the capture stage. It can be expressed by rates in the quasi-stationary case as follows

$$P_{CN} = \frac{\lambda_\eta^{Kr}}{\lambda_R^{Kr} + \lambda_\eta^{Kr}} - \frac{\lambda_\eta^{Kr}\lambda_R^{Kr}}{\lambda_R^{Kr} + \lambda_\eta^{Kr}} \frac{\tau_\eta - \tau_R}{1.72}. \tag{2}$$

As in Ref. [16] we use a two-dimensional Kramers-type expression (quasi–stationary solution of the Fokker-Planck equation) with the quasi-stationary rates of fusion λ_η^{Kr} and quasi–fission λ_R^{Kr} through the fusion barrier ($B^*_{\rm fus}$) in η and quasi–fission barrier ($B_{\rm qf}$) in R, respectively. The second term in (2) is related to the transient times τ_R and τ_η to reach the quasi–stationary rates along the R and η coordinates ($\tau_R^{-1}, \tau_\eta^{-1} > \lambda_R^{Kr}, \lambda_\eta^{Kr}$) [16].

In the case that the fusion barrier is much higher than the quasi-fission barrier, $B^*_{\rm fus} \gg B_{\rm qf}$, i.e. if the transient time τ_η in η is larger (or equal) than the lifetime t_0 of the initial DNS, we obtain [16]

$$P_{CN} = \frac{\lambda_\eta^{Kr}}{1.72}[\tau_\eta(\exp[t_0/\tau_\eta] - 1) - t_0]. \tag{3}$$

Since the pocket in the nucleus-nucleus potential becomes very shallow ($B_{\rm qf} \approx 0$) in reactions with large $Z_1 \times Z_2$, the lifetime t_0 of the DNS is strongly depressed with increasing bombarding energy $E_{\rm c.m.}$ above the Coulomb barrier. Due to this, the value of P_{CN} in Eq.(3) is smaller than the one in the quasi–stationary regime, given by Eq. (2), which can not be reached in this case [16].

The surviving probability under the evaporation of x neutrons is considered according to [17,26] as

$$W_{sur}(E^*_{CN}, J) \approx P_{xn}(E^*_{CN}, J) \prod_{i=1}^{x} \frac{\Gamma_n(E^*_{CN_i}, J_i)}{\Gamma_n(E^*_{CN_i}, J_i) + \Gamma_f(E^*_{CN_i}, J_i)}. \tag{4}$$

Here, P_{xn} is the probability of realization of the xn channel at the excitation energy E^*_{CN} of the compound nucleus, i the index of evaporation step, Γ_n and Γ_f are the partial widths of neutron emission and fission. $E^*_{CN_i}$ and J_i are the mean values of excitation energy and angular momentum quantum number of the compound nucleus, respectively, at the beginning of step i with $E^*_{CN_1} = E^*_{CN}$ and $J_1 = J$. In the calculation of W_{sur} we used the microscopic corrections of Möller and Nix [27] as fission barriers. The neutron binding energies are also taken from [27].

The barriers $B^*_{\rm fus}$ and $B_{\rm qf}$ are given by the potential energy of the DNS which is calculated as the sum of binding energies B_i of the nuclei (i=1,2) and of the nucleus-nucleus potential $V(R, \eta, J)$ [15–17]:

$$U(R,\eta,J) = B_1 + B_2 + V(R,\eta,J) - [B_{12} + V'_{rot}(J)]. \quad (5)$$

The shell effects are included in the binding energies. The isotopic composition of the nuclei forming the DNS is obtained with the condition of a N/Z-equilibrium in the system. The value of $U(R,\eta,J)$ is normalized to the energy of the rotating compound nucleus by $B_{12} + V'_{rot}$. Deformation effects are taken into account in the calculation of the potential energy surface [17]. The heavy nuclei in the DNS, which are deformed in the ground state, are treated with the parameters of deformation taken from Ref. [28]. The light nuclei of the DNS are assumed to be deformed only if the energy of their 2^+ state is smaller than 1.5 MeV. As known from experiments on sub–barrier fusion of lighter nuclei, these states are easily populated. For the collision energies considered here, the relative orientation of the nuclei in the DNS follows the minimum of the potential energy during the evolution in η.

The experimentally observed hindrance of the fusion roughly increases with growing Coulomb repulsion between the colliding nuclei, but also their shell structure and isotopic composition play a major role [6,29–31]. In Table 1 we present calculated excess energies above the entrance Coulomb barrier in the DNS model for various reactions and compare them with the surplus of energy extracted from experimental data above the corresponding Bass barriers [32]. In these calculations we did not average the inner fusion barrier $B^*_{\rm fus}$ over all possible orientations of colliding nuclei as we usually do in the calculations of P_{CN} and σ_{ER}, taking approximately the half of the deformation parameters of the nuclei of the entrance channel. The obtained energy thresholds in η are maximal ones. They are not always in good agreement with the data extracted from experiment because these data are not directly measurable but are obtained with model assumptions about P_{CN} and W_{sur}.

As shown in Table 1 the isotopic trends of the DNS model agree with the experimental ones. The energy thresholds for fusion increase and, correspondingly, the fusion probabilities decrease [29,30] when the neutron number of projectile or target deviates more from a magic number in the reactions ^{90}Zr+^{90,92,96}Zr, ^{90,96}Zr+^{100}Mo ^{86}Kr+^{99,102,104}Ru, ^{90,92,94,96}Zr+^{124}Sn and ^{86}Kr+^{130,136}Xe. This effect is simply explained by the deformation of the nuclei in the initial DNS and DNS at the top of the barrier in η and by the shell effects in dependence of the DNS potential energy on η. For example, the value of the energy threshold for fusion, which determines the fusion probability, is larger in the ^{86}Kr+^{130}Xe reaction than in the ^{86}Kr+^{136}Xe reaction [31]. Since in addition the surviving probability W_{sur} is larger in the reaction with ^{136}Xe than in the reaction with ^{130}Xe, there results an experimental difference of about 3 orders of magnitude in σ_{ER} in these reactions [31]. For most reactions, for example, ^{90}Zr+^{90}Zr, ^{100}Mo+^{100}Mo and ^{110}Pd+^{110}Pd, we obtained evaporation residue cross sections with the values of P_{CN} of the DNS model which are in good agreement with the experimental cross sections [15,16]. In contrast, models which treat fusion as a motion in R, give an incorrect isotopic trend of P_{CN}. In these models P_{CN} always increases with the neutron number above the nearest closed shell [6,32] because an increasing deformation of the nuclei in the entrance channel effectively lowers the barrier.

Since the evaporation residue cross section increases with the number of neutrons in all reactions listed in Table 1, the value of W_{sur} has to grow faster than P_{CN} decreases. In fusion reactions leading to actinides, for example in the ^{66,76}Zn+^{174}Yb reaction, the increase of W_{sur} with the neutron number of the system is stronger than the decrease of P_{CN} This effect, shown in Fig. 1 for reactions ^{A}Zn+^{174}Yb, gives a certain preference for neutron-rich projectiles in producing actinides. Note that the numbers of neutrons in the nuclei ^{66}Zn and

^{76}Zn are close to different magic numbers.

Fusion probabilities in symmetric and almost symmetric reactions with heavy nuclei like ^{124,132}Sn and ^{136,142}Xe strongly depend on the model of fusion. For example, in an adiabatic treatment, where the fusion is mainly described by the dynamics in the relative distance coordinate with an increasing neck, we found $P_{CN} \approx 10^{-6}$ and $\sigma_{ER} \approx$30pb for the reaction ^{132}Sn + ^{132}Sn$\rightarrow^{261}$Fm+3n. In the DNS model the values of P_{CN} and, correspondingly, σ_{ER} are about three orders of magnitude smaller. According to the DNS concept, cross sections for the synthesis of the heaviest elements in nearly symmetric reactions are very small due to small fusion probabilities, for example, in the reactions ^{136}Xe + ^{136}Xe$\rightarrow^{272}$Hs, ^{142}Xe + ^{150,154}Nd$\rightarrow^{292,296}$114, ^{132}Sn + ^{160}Gd$\rightarrow^{292}$114 and ^{137}Te + ^{158}Sm$\rightarrow^{295}$114. Experimental data on symmetric reactions with stable and radioactive beams could help to prove the DNS model for the fusion process and would give information about the time for the transition from the diabatic to adiabatic regime (the time of suppression of the structure forbiddenness for melting of nuclei [20]).

In contrast to other models, the optimal excitation energy E^*_{CN} of the compound nucleus and evaporation residue cross section σ_{ER} in cold fusion reactions with stable projectiles are reproduced in the DNS concept [17]. These results are listed in Table 2 for reactions leading to the Fm element and Pb- and Bi-based reactions. The evaporation residue cross sections are compared with the experimental data of Refs. [1,33]. All other cross sections are predictions of the present version of the DNS model. Figs. 2a) and 2b) show the fusion probabilities and the optimal excitation energies of the compound nuclei, respectively, for ^{208}Pb, ^{209}Bi($^A X, 1n$) reactions.

The values of the optimal excitation energy E^*_{CN} are calculated by applying theoretical Q-values of Refs. [27]. They increase for $Z > 112$. Q-values of Ref. [34] are slightly different for $Z > 113$. As in the case of reactions with heavy nuclei mentioned above, the calculated values of P_{CN} are maximal when the neutron number of the projectile is equal to a magic number, for example, in the reactions ^{82}Ge+^{208}Pb, ^{84}Se+^{208}Pb and ^{86}Kr+^{208}Pb. The decrease of the cold fusion cross section by four orders of magnitude from Z =104 to 112 is mainly caused by a decrease of P_{CN} due to a strong competition between complete fusion and quasi–fission in the DNS (see Fig. 2a)). For the reaction ^{70}Zn+^{208}Pb$\rightarrow^{277}$112+1n, $\sigma_{ER} \approx$1pb is practically on the level of the present experimental possibilities. In reactions ^{74,76}Ge+^{208}Pb$\rightarrow^{283,281}$114+1n we expect a value of σ_{ER} which is smaller than 0.2 pb. The values of σ_{ER} for the Z=116 and 118 elements formed in the ^{84}Se, ^{86}Kr+^{208}Pb reactions are of the order of 0.01 pb (Table 2).

The values of W_{sur} in Table 2 were calculated with the theoretical data of Ref. [27]. One can see that characteristic values of W_{sur} are about $10^{-3} - 10^{-4}$ for nuclei with Z=104–113 and about 10^{-2} for nuclei with Z=114, 116 and 118. The proton magic number 114 in the region of the stability island [27,34,35] leads to a larger increase of W_{sur}. The large W_{sur} of the nuclei ^{292}114, ^{294}116 and ^{296}118 arises due to the fact that the neutron number in these nuclei is equal to the theoretically predicted magic number N=178 [27,34]. When the number of neutrons deviates from this magic number, W_{sur} decreases. The surviving probabilities in the reactions ^{70}Zn+^{208}Pb and ^{74}Ge+^{208}Pb were calculated with the data of Ref. [34] because W_{sur} becomes unrealistically small with the data of Ref. [27] (about two orders of magnitude in comparison to the neighbouring nuclei). Using the microscopical corrections and neutron binding energies from Ref. [34] instead of Ref. [27] we obtained even smaller cross sections σ_{ER} of 50, 5 and 0.8 fb for the reactions with the projectiles

^{76}Ge, ^{82}Se and ^{86}Kr on ^{208}Pb, respectively. With the fission characteristics of Ref. [35] we get evaporation residue cross sections σ_{ER} which are again smaller than the latter ones. In conclusion the cross sections in Table 2 are optimistic estimates.

Let us consider whether the expected values of evaporation residue cross sections are larger with radioactive projectiles. In the Pb-based reactions with neutron-rich nuclei ^{70,74,78}Ni, ^{80}Zn, $^{78-86}$Ge, $^{84-92}$Se and $^{88-92}$Kr the inner fusion barrier B^*_{fus} in mass asymmetry varies between 12 and 22 MeV. In order to overcome this barrier, the initial DNS must have excitation energies which lead to an excited compound nucleus with the possibility of an $1n$ or $2n$ emission. The calculated cross sections for some possible reactions are presented in Table 2. Bombarding energies near the Coulomb barrier lead to maximal evaporation residue cross sections. In these reactions the increase of W_{sur} is compensated by a decreasing fusion probability P_{CN} and the value of σ_{ER} depends weakly on the isotopic composition of the colliding nuclei. The values of P_{CN} and W_{sur} for the reactions ^{A}Ni+^{208}Pb and ^{A}Ge+^{208}Pb are presented in Fig. 3 as functions of A. The calculations were performed with the same parameters as used for the stable projectiles and are in good agreement with experimental data (Table 2) [1,17]. Due to deformation effects and binding energies of the nuclei in the DNS, the dependence of P_{CN} on A can have some minima and maxima.

The yield of the element $Z = 110$ results larger in the ^{78}Ni+^{208}Pb reaction than in the ^{62,64}Ni+^{208}Pb reactions. In the ^{70,74}Ni+^{208}Pb reactions the values of σ_{1n} are close to the experimental value of $\sigma_{1n} = 3.5^{+2.7}_{-1.8}$ pb of the ^{62}Ni+^{208}Pb reaction. In the ^{70,74}Ni+^{208}Pb reactions the cross sections σ_{2n} are about 4 times smaller than σ_{1n} due to smaller values of σ_c and W_{sur}. In spite of the large values of W_{sur} in the reactions ^{84,86}Ge+^{208}Pb, ^{86,88,90,92}Se+^{208}Pb and ^{88,90,92}Kr+^{208}Pb, the corresponding values of σ_{ER} are expected to be smaller than 0.1 pb due to the very small values of P_{CN} (Table 2 and Fig. 3).

In spite of the expected relatively small yields for neutron–rich superheavies the larger lifetime of these nuclei will allow a detailed study of their properties. The lifetime of molecular–type configurations with an initial DNS in the entrance channel can be studied with beams of radioactive nuclei. In reactions with neutron–rich nuclei, a neutron emission can occur out of the DNS besides a possible quasi-fission because the characteristic emission time becomes comparable with the fusion time. This process decreases the excitation energy of the DNS and the fusion probability. The effect of neutron emission from the DNS is expected to be important for energies larger than the energy in the $3n$ channel. With a neutron emission from the DNS the fusion process is more complex and has to be studied.

Intensive beams of neutron-rich nuclei are very useful for producing heavy actinides, e.g. Fm as listed in Table 2. In the Pb-based reactions the use of neutron-rich projectiles leads to values of σ_{ER} comparable with evaporation residue cross sections for reactions with the stable projectiles. More asymmetric reactions with radioactive beams could be more useful in the production of superheavies.

We thank Profs. D.Habs, R.V.Jolos, G.Münzenberg, V.V.Volkov, Drs. E.A.Cherepanov, S.P.Ivanova and A.K.Nasirov for fruitful discussions and suggestions. G.G.A. is grateful to Alexander von Humboldt-Stiftung (Bonn) for support. This work was supported in part by DFG and RFBR.

REFERENCES

[1] S.Hofmann, Rep. Prog. Phys. 61 (1998) 636.
[2] G.Münzenberg, Phil. Trans. R. Soc. Lond. A 356 (1998) 2083.
[3] Yu.Ts.Oganessian et al., Eur. Phys. J A 5 (1999) 63; Preprint JINR, E7-99-53 (1998); A.V.Yeremin, V.K.Utyonkov and Yu.Ts.Oganessian *in* AIP Conf. Proc. 425 (1998) 16.
[4] D.Habs et al., Nucl. Phys. A 616 (1997) 39c.
[5] G.Münzenberg et al., *in* Superheavy elements. Munich Accelerator for Fission Fragments. Physics Case and Technical Description, eds. D.Habs et al. (Munich, 1998) 5.
[6] K.H.Schmidt and W.Morawek, Rep. Prog. Phys. 54 (1991) 949.
[7] A.Sandulescu, R.K.Gupta, W.Scheid and W.Greiner, Z. Phys. A 283 (1977) 217.
[8] W.J. Swiatecki, Phys. Scripta 24 (1981) 113.
[9] P. Fröbrich, Phys. Rep. 116 (1984) 337.
[10] G.Royer and B.Remaud, Nucl. Phys. A 444 (1985) 477.
[11] C.E.Aguiar, V.C.Barbosa and R.Donangelo, Nucl. Phys. A 517 (1990) 205.
[12] Y.Aritomo, T.Wada, M.Ohta and Y.Abe, Phys. Rev. C 59 (1999) 796.
[13] G.G.Adamian, N.V.Antonenko, S.P.Ivanova and W.Scheid, Nucl. Phys. A 646 (1999) 29.
[14] V.V.Volkov, *in* Proc. Int. School-Seminar on Heavy Ion Physics, Dubna, 1986 (JINR, Dubna, 1987) p.528; Izv. AN SSSR ser. fiz. 50 (1986) 1879.
[15] N.V.Antonenko, E.A.Cherepanov, A.K.Nasirov, V.B.Permjakov and V.V.Volkov, Phys. Lett. B 319 (1993) 425; Phys. Rev. C 51 (1995) 2635.
[16] G.G.Adamian, N.V.Antonenko and W.Scheid, Nucl. Phys. A 618 (1997) 176; G.G.Adamian, N.V.Antonenko, W.Scheid and V.V.Volkov, Nucl. Phys. A 627 (1997) 361.
[17] G.G.Adamian, N.V.Antonenko, W.Scheid and V.V.Volkov, Nucl. Phys. A 633 (1998) 409; Nuovo Cimento A 110 (1997) 1143.
[18] R.V. Jolos, A.K. Nasirov and A.I. Muminov, Eur. Phys. J. A 4 (1999) 245;
[19] E.A.Cherepanov, Preprint JINR, E7-99-27 (1999).
[20] G.G.Adamian, N.V.Antonenko and Yu.M.Tchuvil'sky, Phys. Lett. B 451 (1999) 289.
[21] Yu.F.Smirnov and Yu.M.Tchuvil'sky, Phys. Lett. B 134 (1984) 25; O.F.Nemetz, V.G.Neudatchin, A.T.Rudchik, Yu.F.Smirnov and Yu.M. Tchuvil'sky, Nucleonic clusters in nuclei and the many-nucleon transfer reactions (Kiev: Naukova Dumka, 1988).
[22] A.Diaz-Torres, N.V.Antonenko and W.Scheid, Nucl. Phys. A 652 (1999) 61.
[23] J.Töke et al., Nucl. Phys. A 440 (1985) 327.
[24] D.J.Hinde, et al., Phys. Rev. C 53 (1996) 1290.
[25] P.Reiter et al., Phys. Rev. Lett. 82 (1999) 509.
[26] E.A.Cherepanov, *in* Proc. Int. Symp. on In Beam Nuclear Spectropscopy, Debrecen, 1984, p.499; E.A. Cherepanov and A.S. Iljinov, Nucleonika 25 (1980) 611.
[27] P.Möller and R.Nix, At. Data Nucl. Data Tables 39 (1988) 213
[28] S.Raman et al., At. Data Nucl. Data Tables 36 (1987) 1.
[29] A.B. Quint et al., Z. Phys. A 346 (1993) 119.
[30] C.-C. Sahm et al., Z. Phys. A 319 (1984) 113; Nucl. Phys. A 441 (1985) 316.
[31] Yu.Ts.Oganessian et al., FLNR Scientific Report 1995-1996 (JINR, Dubna, 1997) 62.
[32] D.Berdichevsky et al., Nucl. Phys. A 499 (1989) 609.
[33] H.Gäggeler et al., Z. Phys. A 316 (1984) 291.

[34] P.Möller et al., At. Data Nucl. Data Tables 59 (1995) 185.
[35] S.Cwiok and A.Sobiczewski, Z. Phys. A 342 (1992) 203; R.Smolanczuk, J.Skalski and A.Sobiczewski, Phys. Rev. C 52 (1995) 1871; R.Smolanczuk, Phys. Rev. C 59 (1999) 2634.

TABLES

TABLE I. Calculated maximal energy excess ΔE^{th} above the entrance Coulomb barrier in the DNS model and the surplus of energy ΔB^{exp} above the Bass barrier extracted from experimental data [32]. The number of valence neutron particles or holes to the nearest closed shell in the projectile or target is denoted by ΔN.

Reactions	ΔN	ΔE^{th} (MeV)	ΔB^{exp} (MeV)	Reactions	ΔN	ΔE^{th} (MeV)	ΔB^{exp} (MeV)
^{86}Kr+^{92}Mo→^{178}Pt	0	0.0	$1.4^{+1.0}_{-1.0}$	^{98}Mo+^{100}Mo→^{198}Po	6	12.6	$14.1^{+1.0}_{-1.0}$
^{86}Kr+^{100}Mo→^{186}Pt	8	2.0	$4.3^{+2.0}_{-2.0}$	^{100}Mo+^{100}Mo→^{200}Po	8	10.3	$12.2^{+0.5}_{-0.5}$
^{86}Kr+^{99}Ru→^{185}Hg	5	3.6	$3.1^{+1.2}_{-1.2}$	^{100}Mo+^{104}Ru→^{204}Rn	10	12.7	$23.0^{+1.1}_{-1.1}$
^{86}Kr+^{102}Ru→^{188}Hg	8	5.2	$6.5^{+1.3}_{-1.3}$	^{100}Mo+^{110}Pd→^{210}Ra	14	13.7	$29.0^{+1.2}_{-1.2}$
^{86}Kr+^{104}Ru→^{190}Hg	10	5.8	$7.2^{+1.3}_{-1.3}$	^{90}Zr+^{124}Sn→^{214}Th	0	6.1	$20.3^{+4.0}_{-4.0}$
^{90}Zr+^{90}Zr→^{180}Hg	0	2.9	$0.0^{+0.5}_{-0.5}$	^{92}Zr+^{124}Sn→^{216}Th	2	6.6	$20.8^{+4.0}_{-3.0}$
^{90}Zr+^{92}Zr→^{182}Hg	2	4.0	$4.2^{+0.5}_{-0.5}$	^{94}Zr+^{124}Sn→^{118}Th	4	8.8	$22.7^{+5.0}_{-3.0}$
^{90}Zr+^{96}Zr→^{186}Hg	6	4.6	$5.1^{+0.5}_{-0.5}$	^{96}Zr+^{124}Sn→^{220}Th	6	12.5	$26.7^{+5.0}_{-3.0}$
^{96}Zr+^{96}Zr→^{192}Hg	6	6.9	$4.2^{+1.2}_{-1.2}$	^{86}Kr+^{130}Xe→^{116}Th	6	7.8	
^{90}Zr+^{100}Mo→^{190}Pb	0	5.5	$5.1^{+1.0}_{-1.0}$	^{86}Kr+^{136}Xe→^{222}Th	0	5.0	
^{92}Zr+^{100}Mo→^{192}Pb	2	7.0	$5.8^{+1.0}_{-1.0}$	^{110}Pd+^{110}Pd→^{220}U	14	20.9	
^{96}Zr+^{100}Mo→^{196}Pb	6	8.8	$9.5^{+1.0}_{-1.0}$	^{124}Sn+^{124}Sn→^{248}Fm	8	23.2	
^{92}Mo+^{100}Mo→^{192}Po	0	11.8	$13.0^{+2.0}_{-2.0}$	^{132}Sn+^{132}Sn→^{264}Fm	0	30.7	
^{94}Mo+^{100}Mo→^{194}Po	2	14.9	$16.3^{+1.0}_{-1.0}$	^{130}Xe+^{130}Xe→^{260}Hs	6	37.7	
^{96}Mo+^{100}Mo→^{196}Po	4	8.2	$10.4^{+1.0}_{-1.0}$	^{136}Xe+^{136}Xe→^{272}Hs	0	33.1	

TABLE II. Excitation energy E^*_{CN} of compound nucleus, fusion probability P_{CN}, capture cross section σ_c, surviving probability W_{sur}, and theoretical σ^{th}_{ER} and experimental σ^{exp}_{ER} evaporation residue cross sections for reactions leading to the Fm nucleus and Pb-based reactions. The experimental data are taken from Refs. [33] and [1] (cold fusion).

Reactions	E^*_{CN} (MeV)	P_{CN}	σ_c (mb)	W_{sur}	σ^{th}_{ER}	σ^{exp}_{ER}
^{66}Zn+^{174}Yb$\rightarrow^{238}$Fm+2n	26.0	4×10^{-2}	9.6	8.0×10^{-7}	0.3 nb	
^{76}Zn+^{174}Yb$\rightarrow^{248}$Fm+2n	23.0	2×10^{-3}	8.8	6.0×10^{-4}	10.6 nb	
^{76}Ge+^{170}Er$\rightarrow^{244}$Fm+2n	24.6	5×10^{-4}	8.4	3.0×10^{-4}	1.3 nb	$1.6^{+1.3}_{-1.6}$ nb
^{50}Ti+^{208}Pb$\rightarrow^{257}$ 104 + 1n	16.1	3×10^{-2}	5.3	9×10^{-5}	14.3 nb	$10^{+1.3}_{-1.3}$ nb
^{50}Ti+^{209}Bi$\rightarrow^{258}$ 105 + 1n	16.2	3×10^{-3}	5.2	3×10^{-4}	4.7 nb	$4^{+1.3}_{-1.6}$ nb
^{54}Cr+^{208}Pb$\rightarrow^{261}$ 106 + 1n	16.0	9×10^{-4}	4.6	1×10^{-4}	0.4 nb	$0.5^{+0.14}_{-0.14}$ nb
^{54}Cr+^{209}Bi$\rightarrow^{262}$ 107 + 1n	15.9	2×10^{-4}	4.5	3×10^{-4}	270 pb	163^{+34}_{-34} pb
^{58}Fe+^{208}Pb$\rightarrow^{265}$ 108 + 1n	15.5	3×10^{-5}	4.0	4×10^{-4}	48 pb	$65.8^{+7.5}_{-7.5}$ pb
^{58}Fe+^{209}Bi$\rightarrow^{266}$ 109 + 1n	15.7	6×10^{-6}	4.0	5×10^{-4}	12 pb	$8.8^{+3.3}_{-3.3}$ pb
^{62}Ni+^{208}Pb$\rightarrow^{269}$ 110 + 1n	12.3	4.5×10^{-6}	3.5	5×10^{-4}	7 pb	$3.5^{+2.7}_{-1.8}$ pb
^{64}Ni+^{208}Pb$\rightarrow^{271}$ 110 + 1n	10.7	1×10^{-5}	3.4	5×10^{-4}	17 pb	15^{+9}_{-6} pb
^{70}Ni+^{208}Pb$\rightarrow^{277}$ 110 + 1n	13.5	7×10^{-8}	3.1	5×10^{-3}	1.1 pb	
^{74}Ni+^{208}Pb$\rightarrow^{281}$ 110 + 1n	15.0	6×10^{-8}	3.0	2×10^{-2}	3.6 pb	
^{78}Ni+^{208}Pb$\rightarrow^{284}$ 110 + 2n	17.5	2×10^{-7}	3.0	6×10^{-2}	36 pb	
^{64}Ni+^{209}Bi$\rightarrow^{272}$ 111 + 1n	10.5	2×10^{-6}	3.4	6×10^{-4}	4.1 pb	$3.5^{+4.6}_{-2.3}$ pb
^{70}Zn+^{208}Pb$\rightarrow^{277}$ 112 + 1n	9.8	1×10^{-6}	3.0	6×10^{-4}	1.8 pb	$1.0^{+1.3}_{-0.7}$ pb
^{80}Zn+^{208}Pb$\rightarrow^{286}$ 112 + 2n	15.7	7×10^{-9}	2.6	1×10^{-1}	1.8 pb	
^{68}Zn+^{209}Bi$\rightarrow^{276}$ 113 + 1n	9.6	1×10^{-6}	2.9	1×10^{-4}	290 fb	
^{70}Zn+^{209}Bi$\rightarrow^{278}$ 113 + 1n	10.6	4×10^{-7}	2.9	2×10^{-4}	232 fb	$<$600 fb
^{74}Ge+^{208}Pb$\rightarrow^{281}$ 114 + 1n	12.5	2×10^{-8}	2.5	2×10^{-3}	100 fb	
^{76}Ge+^{208}Pb$\rightarrow^{283}$ 114 + 1n	12.4	4×10^{-9}	2.5	2×10^{-2}	200 fb	
^{78}Ge+^{208}Pb$\rightarrow^{285}$ 114 + 1n	14.2	5×10^{-10}	2.1	2×10^{-2}	21 fb	
^{82}Ge+^{208}Pb$\rightarrow^{289}$ 114 + 2n	16.3	1×10^{-9}	2.0	1×10^{-1}	200 fb	
^{84}Ge+^{208}Pb$\rightarrow^{291}$ 114 + 2n	18.5	2×10^{-10}	2.0	2×10^{-1}	80 fb	
^{86}Ge+^{208}Pb$\rightarrow^{294}$ 114 + 2n	20.4	4×10^{-10}	2.0	4×10^{-2}	32 fb	
^{82}Se+^{208}Pb$\rightarrow^{289}$ 116 + 1n	13.8	4×10^{-10}	1.9	2×10^{-2}	15 fb	
^{84}Se+^{208}Pb$\rightarrow^{291}$ 116 + 1n	14.6	7×10^{-10}	1.8	2×10^{-2}	25 fb	
^{86}Se+^{208}Pb$\rightarrow^{293}$ 116 + 2n	14.8	1×10^{-10}	1.8	6×10^{-2}	11 fb	
^{88}Se+^{208}Pb$\rightarrow^{295}$ 116 + 2n	15.0	8×10^{-11}	1.8	2×10^{-2}	2.9 fb	
^{90}Se+^{208}Pb$\rightarrow^{297}$ 116 + 2n	14.8	1×10^{-10}	1.8	2×10^{-2}	3.6 fb	
^{92}Se+^{208}Pb$\rightarrow^{299}$ 116 + 2n	20.2	1.5×10^{-10}	1.8	6×10^{-3}	1.7 fb	
^{84}Kr+^{208}Pb$\rightarrow^{291}$ 118 + 1n	12.5	5×10^{-11}	1.7	2×10^{-2}	1.7 fb	
^{86}Kr+^{208}Pb$\rightarrow^{293}$ 118 + 1n	13.3	1.5×10^{-10}	1.7	2×10^{-2}	5.1 fb	
^{88}Kr+^{208}Pb$\rightarrow^{295}$ 118 + 1n	12.0	3×10^{-11}	1.7	8×10^{-2}	4.1 fb	
^{90}Kr+^{208}Pb$\rightarrow^{297}$ 118 + 1n	13.1	1.5×10^{-11}	1.6	5×10^{-2}	1.2 fb	
^{92}Kr+^{208}Pb$\rightarrow^{299}$ 118 + 1n	12.4	1.5×10^{-11}	1.6	4×10^{-2}	1.0 fb	

FIGURES

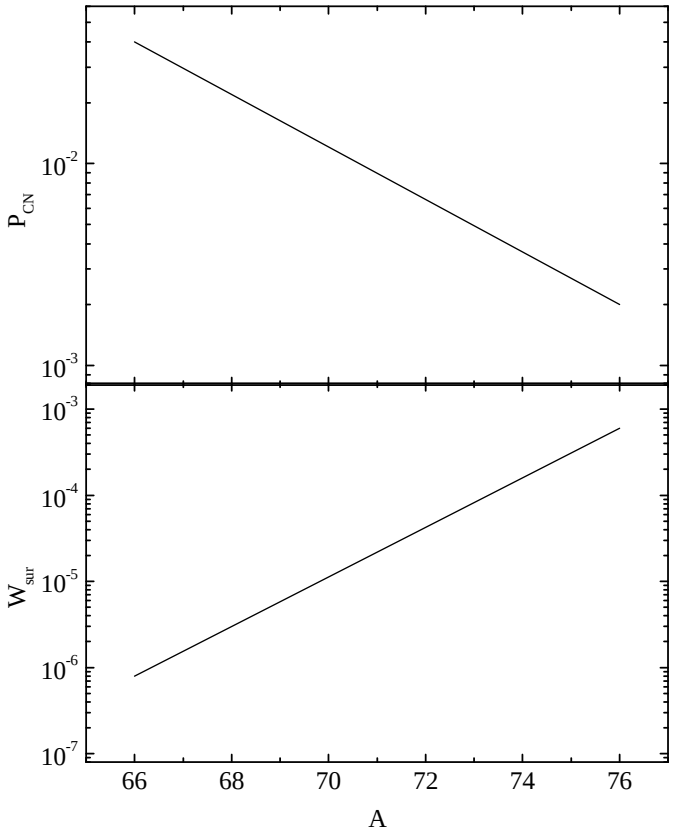

Fig.1 Adamian et al.

FIG. 1. Fusion (P_{CN}) and surviving (W_{sur}) probabilities as functions of mass number A of the projectile in reactions ^{A}Zn+^{174}Yb at bombarding energies supplying the maximum yield of evaporation residues.

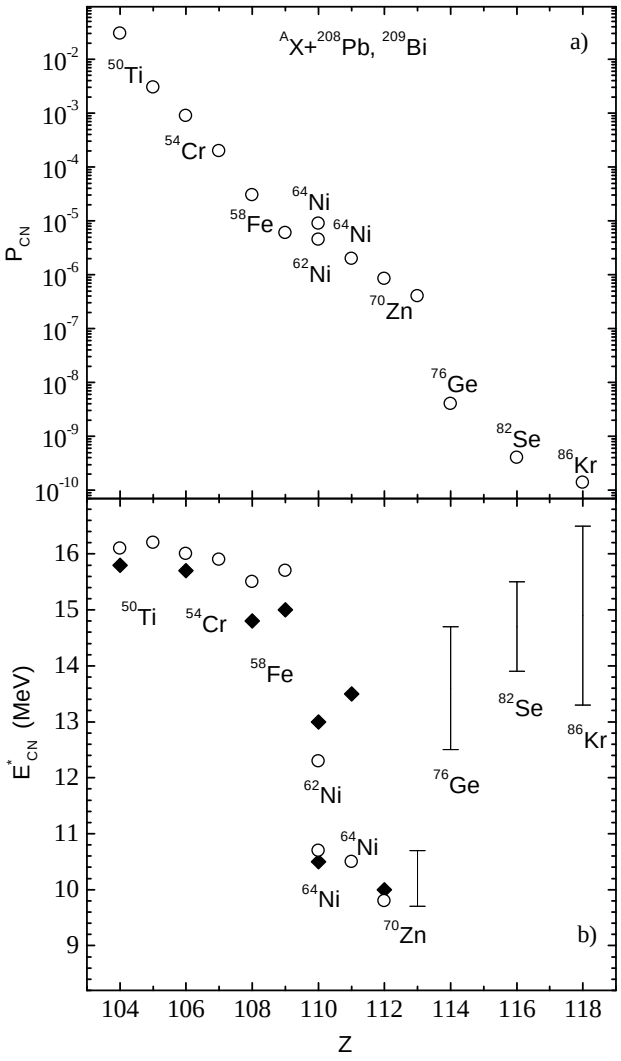

Fig.2 G.G.Adamian et al.

FIG. 2. a) Calculated fusion probabilities P_{CN} for cold fusion in (HI,1n) reactions for the projectiles indicated (open circles). The experimental data [1,2] are shown by solid diamonds. For the compound nuclei with Z=104-112, the calculations were performed with Q-values from Ref. [27]. b) Optimal excitation energies of the compound nuclei. For the nuclei with Z=113,114,116 and 118, the lower and upper limits of bars were calculated with Q-values from Ref. [27] and Ref. [34], respectively.

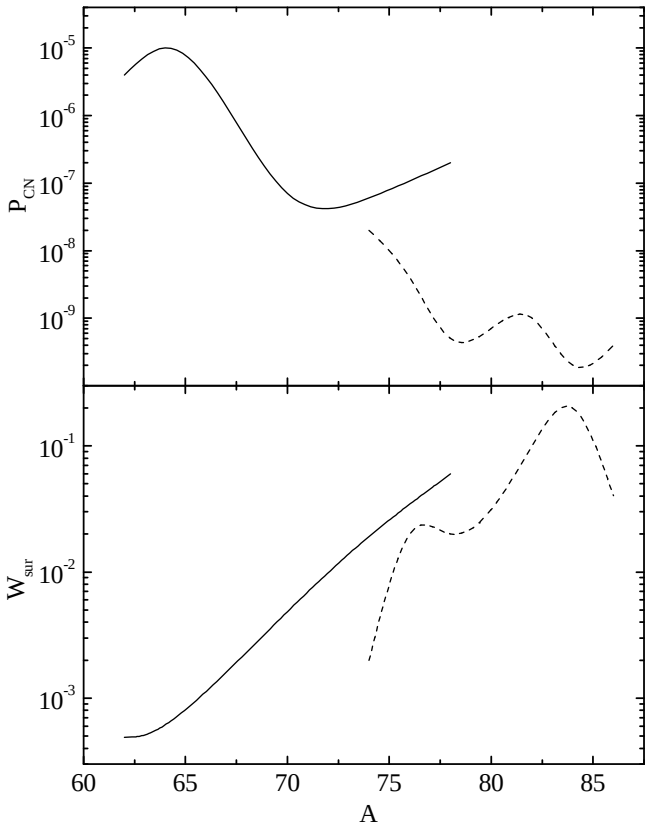

Fig.3 Adamian et al.

FIG. 3. The same as in Fig. 1 for the reactions ^{A}Ni+^{208}Pb (solid lines) and ^{A}Ge+^{208}Pb (dashed lines).